



Analysis and improvement of material flow during extrusion process using spreading pocket die for large-size, flat-wide, and multi-ribs profile

Zhiwen Liu^{1,2} · Luoxing Li³ · Guan Wang⁴ · Jie Yi³

Received: 27 September 2019 / Accepted: 20 January 2020 / Published online: 28 January 2020
© Springer-Verlag London Ltd., part of Springer Nature 2020

Abstract

Spreading extrusion is an advanced technology to produce the solid aluminum profiles with large-size, flat-wide, and thin-walled structures. Currently, little research has been reported on the hot extrusion process through spreading pocket die for manufacturing these kinds of aluminum profiles. It is a challenging task for die engineers to control the billet through die cavity with a uniform velocity. Reasonable structure design for spreading pocket die can eliminate extrusion defects and improve the performance of extrudate. In this paper, virtual tryout of spreading extrusion process for a large-size, flat-wide, and multi-ribs aluminum profile was performed through arbitrary Lagrangian-Eulerian simulation. Firstly, spreading pocket die was designed based on the theory of metal plastic flowing. The uniformity of flow velocity distribution on the cross-section of die exit was evaluated quantitatively through standard deviation calculation. Then, a series of structure modifications for the spreading pocket die was proposed to improve material flow during die cavity based on the simulated results. Thirdly, a synthetical comparison of extrusion formability for the modified and initial spreading pocket dies was carried out, including the metal flow behavior, exit temperature, residual stress of extrudate, and peak extrusion force. Finally, the modified extrusion dies were manufactured, and corresponding extrusion experiment was performed to verify the effectiveness and reliability of numerical simulations. The key design points of spreading pocket die for large-size, flat-wide, and multi-ribs aluminum profile were concluded.

Keywords Large-size and flat-wide profile · Multi-ribs · Spreading pocket die · Material flow balance · Arbitrary Lagrangian-Eulerian simulation

1 Introduction

With the rapid development of science, technology, and global economy, aluminum profiles are developing towards the direction of large-size and integration, thin-walled and flat-wide

structure, and high-dimensional accuracy. To realize the light-weight design, energy conservation and emission reduction of vehicles, such as automotive, subway, high-speed train, and city bus, aluminum profiles have been widely used in many structural parts of the abovementioned vehicles [1–3]. The traditional design of assembly structure by using several processed classical components can be replaced with an integral structure; thus, the number of welded joints is minimized and the smoothness and reliability of vehicles can be greatly improved. It can be predicted that in the near future, large-size and flat-wide solid profiles (Fig. 1) will play an increasingly important role in the application of vehicles.

Owing to the complex structure characteristics of flat-wide and multi-ribs profile, it is not practical to extrude the billet directly through the flat-faced die to form the large-size profiles. In such circumstances, the spreading pocket die is designed and used to manufacture this kind of aluminum profile [4–6]. The goal of manufacturing large section profile with small extruder can be realized by using spreading pocket

✉ Zhiwen Liu
liuzhiwen1008@163.com

¹ College of Mechanical Engineering, University of South China, Hengyang 421001, China

² Cooperative Innovation Center for Nuclear Fuel Cycle Technology and Equipment, University of South China, Hengyang 421001, China

³ State Key Laboratory of Advanced Design and Manufacture for Vehicle Body, Hunan University, Changsha 410082, China

⁴ College of Mechanical Engineering, Ningxia University, Yinchuan 750021, China

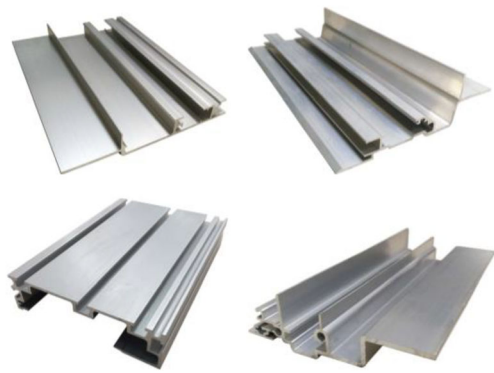


Fig. 1 Typical aluminum profiles with large-size, flat-wide, and thin-walled structures

die, and the production and die costs can be reduced. The spreading pocket die consist of two parts: spreading ring and pocket die. During the spreading extrusion process, the billet is first pre-deformed through the spreading ring; consequently, the billet is spread with an external diameter which is larger than the container diameter. Then, the spreading billet material is further allocated through the pocket to obtain a workpiece similar to the cross-section shape of profile. Finally, the workpiece is extruded through the flat-faced die to form the required profile. The difference between the extrusion productions for large-size solid profile and simple profile is that the billet diameter required for large-size profile is larger. With the increase of billet diameter, the differences of hydrostatic pressure and material flow velocity between the center and edge of the container and spreading pocket die increase. Therefore, it is very difficult to control the billet material through the extrusion dies with uniform flow velocity at die exit.

The traditional design methods of extrusion dies are mainly dependent on the experience and expertise of the die designers [7, 8] or upper bound analysis method [9, 10]. The newly designed dies usually need several extrusion experiments and repairs before it can be put into use, resulting in the prolonging of production cycles of products and the reducing of product eligibility rate. In contrast, finite element (FE) method can simulate the complex extrusion process and obtain a large amount of results of physical quantities, such as extrusion load, material flow velocity, temperature, and stress fields [11–15]. Thus, it has become the most effective tool to study extrusion process

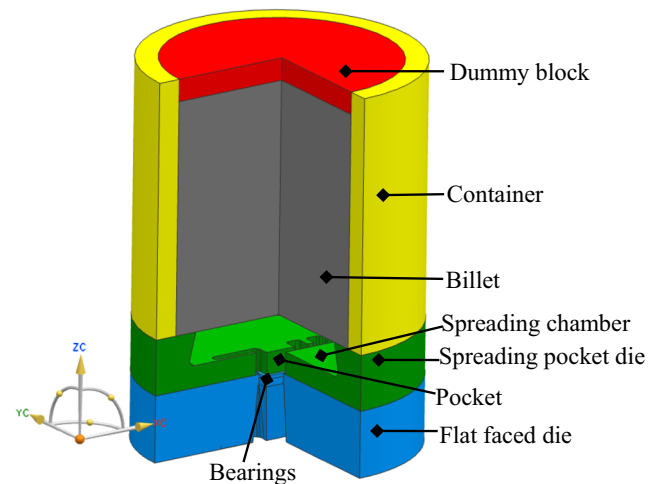


Fig. 3 Schematic drawing of spreading die extrusion assembly

and optimize die structures for the complex and large-size aluminum profiles. Liao et al. [16] have developed a multi-output porthole extrusion die to obtain a better material flow balance for AA6060 aluminum tubes. Pan et al. [17] proposed an inlet structure design method of arc-shaped die to alleviate the hydrostatic pressure on porthole die for large hollow profile. Zhang et al. [18] investigated the material flow during porthole extrusion process through cylinder container and spread die for large-size and hollow aluminum profiles. Imamura et al. [19] investigated the effect of spread ring height and shape on the material flow behavior during spreading extrusion as well as front end shape and discard macrostructure of profile. Yan et al. [20] proposed an approach for the optimal design of technological variables and configured a reasonable die-hole layout for a simple profile extrusion process, which integrates a FE simulation technique, artificial neural network, and genetic algorithms. Abrinia et al. [21] proposed a new analytical formulation to predict the extrusion load and die design process for the profile cross-section with larger dimension than initial billet diameter. Liu et al. [22] studied the extrusion processes of three spread dies with different entrance shapes used generally in the real extrusion production for large-scale aluminum panel through FE simulations. Zhou et al. [23] designed a series of single-bearing dies with pockets of different sizes, volumes, and shapes and have investigated their effects on material flow by

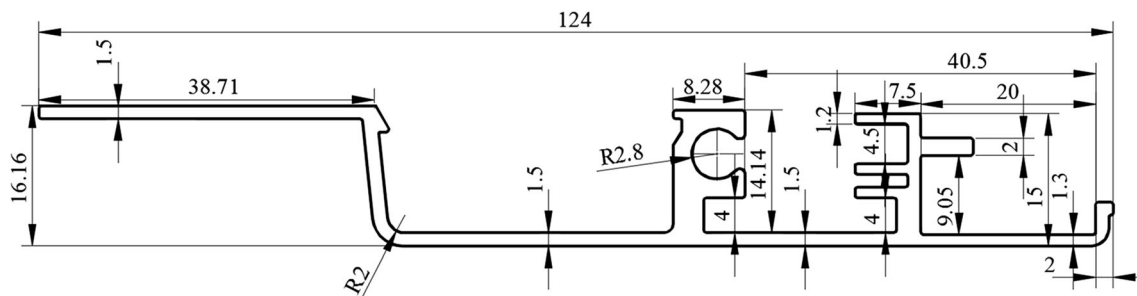
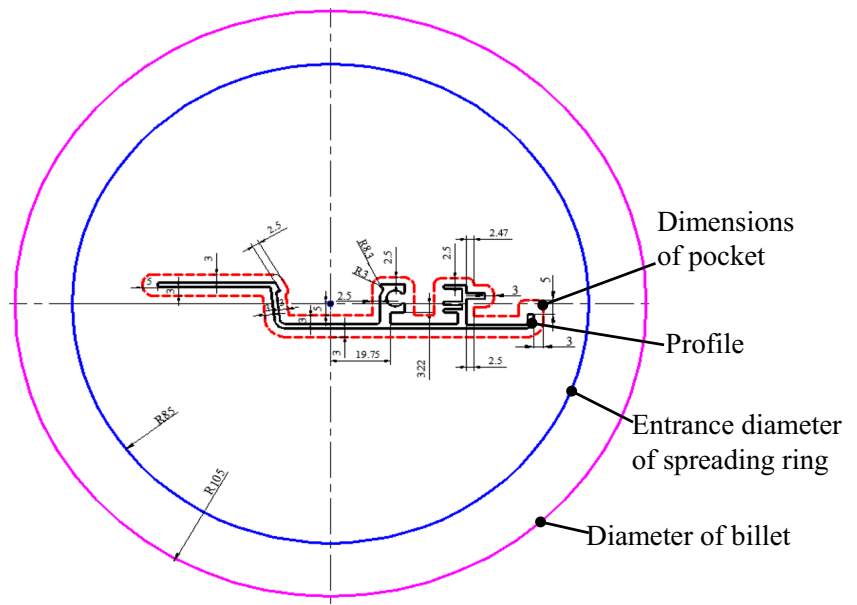


Fig. 2 Cross-section shape and main dimensions of extruded aluminum profile (unit:mm)

Fig. 4 The geometric shapes and dimensions of spreading chamber and pocket for the initial die scheme (unit:mm)



using FE simulations with experimental verifications. Zhao et al. [24] have adopted the response surface method and mesh deformation technique for automatically optimizing the feeder chamber of extrusion die for an aluminum alloy beam.

As can be seen from the above literature, many researches have been carried out to investigate the porthole or pocket dies extrusion process for aluminum profiles. However, little research has been reported on the hot extrusion process using spreading pocket die for manufacturing the large-scale and flat-wide solid aluminum profiles; thus, there is few related literature to be referred for real extrusion productions. In this work, taking a large-size, flat-wide, and multi-ribs aluminum profile as an example, a spreading pocket die was designed based on the theory of metal plastic flowing, and the virtual tryout of spread extrusion process was performed through FE simulation. The uniformity of flow velocity distribution on the cross-section of die exit was evaluated quantitatively by calculating the standard deviation of the velocity (SDV). To optimize material flow during die cavity, pocket steps, the shape and size of pockets and bearing lengths will be modified reasonably. After a series of modifications, a synthetical comparison of extrusion formability for the initial and optimized dies was carried out, including the metal flow behavior, exit

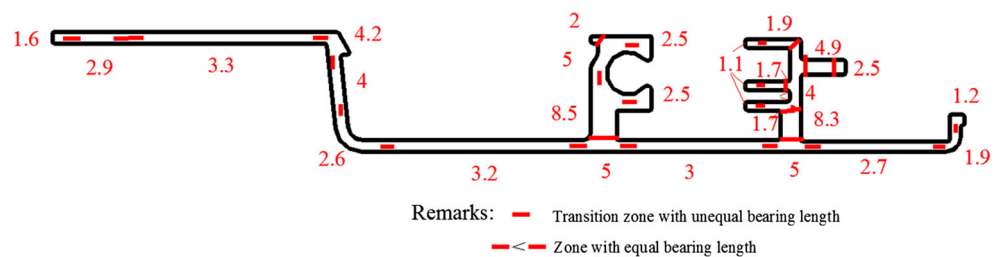
temperature, residual stresses of extrudate, and extrusion force. Finally, the modified extrusion dies were manufactured, and corresponding extrusion experiment was performed to verify the reliability of die design based on FE simulations.

2 Design of spreading pocket die and establishing of FE model

2.1 Design of spreading pocket die and geometry modeling

The research object in the present study is a typical large-size, flat-wide, and multi-ribs aluminum profile, which is widely applied in the automotive skylights. Figure 2 shows the cross-section shape and main dimensions of the extruded profile. It can be seen that the profile has a maximum width of 124 mm and a minimum wall thickness of 1.3 mm. The maximum length–width ratio reached to 95.38, which makes it very difficult to extrude the billet through extrusion die with uniform flow velocity. Moreover, the cross-section shape of this profile is very complex. The two main horizontal panels are not in the same straight line with a height of 16.16 mm. There are

Fig. 5 Design of bearing lengths for the initial die scheme (unit:mm)



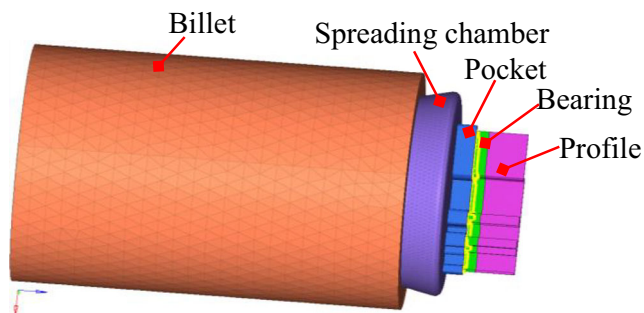


Fig. 6 FE model for simulating the spreading extrusion process

multiple ribs on one main panel, which further increases the difficulty of extrusion process.

Figure 3 shows the schematic drawing of spreading die extrusion assembly. To improve the service life of pocket die and material flow uniformity during extrusion, a spreading pocket die is placed between the container and flat-faced die to form a semi-workpiece with larger diameter than the external diameter of extruded profile. The design principle of spreading pocket die is primarily based on the plastic flowing theory of metal. Figure 4 shows the geometric shapes and dimensions of spreading chamber and pocket for the initial die scheme. In order to prevent the profile twisting and bending caused by the dead-weight of the profile, the large horizontal surface of profile is laid downward in the normal surface of die orifice face to increase the stability of extruded profiles. The centroid of profile coincided with the center of spreading pocket and flat-faced dies. The outer diameter and total height of the extrusion dies are 250 and 110 mm, respectively. There are two important structural parameters, such as spreading angle β and ring thickness H in the design of spring ring. The spreading angle β is given as follows: $H = \frac{B_2 - B_1}{2 \tan \beta}$. B_1 and B_2 are the outlet and entrance diameters of spreading ring, respectively. β is generally less than 30° . The shape of the spreading ring is designed as conical type with an entrance diameter of 170 mm and a spread angle of 15° . More importantly, a pocket with a shape similar to the profile's outline is designed to further balance the material flow before the billet extrudes through the orifice of flat-faced die. The depth of pocket is set to 20 mm and the distances between the pocket edge and die orifices are designed to 3~5 mm based on the positions of orifices away from the die center and wall thicknesses of parts of profile. The die

bearings are arranged at the die orifices to generate different frictional resistances for material flow, and the detailed design scheme is shown in Fig. 5.

2.2 FE modeling of extrusion process using spreading pocket die

There are several algorithms such as update Lagrangian algorithm [5, 6, 13], Euler algorithm [25], and arbitrary Lagrangian-Eulerian (ALE) algorithm [14–18], which have been successfully applied to extrusion simulations. For these algorithms, ALE algorithm can overcome the shortcomings of the updated Lagrangian and Eulerian algorithms; thus, frequent re-meshing ineluctable in update Lagrangian algorithm could be avoided. Besides, the disadvantage of Euler algorithm, especially the difficulty of free surfaces tracking, is also evaded due to the nature of algorithm which is incremental. For the ALE formulation, a referential domain (Ω_ξ) is employed, which is independent on the material domain (Ω_X) and spatial domain (Ω_x). The laws of conservation of mass, momentum, and energy can be expressed as follows:

Law of mass conservation:

$$\frac{\partial \rho}{\partial t} \Big|_{\xi} + \frac{\partial \rho w_i}{\partial \xi_i} = 0 \quad (1)$$

Momentum equation:

$$\rho \frac{\partial v_i}{\partial t} \Big|_{\xi} + \rho w_j \frac{\partial v_i}{\partial \xi_j} = \frac{\partial T_{ji}}{\partial \xi_j} + \rho f_i \quad (2)$$

Energy equation:

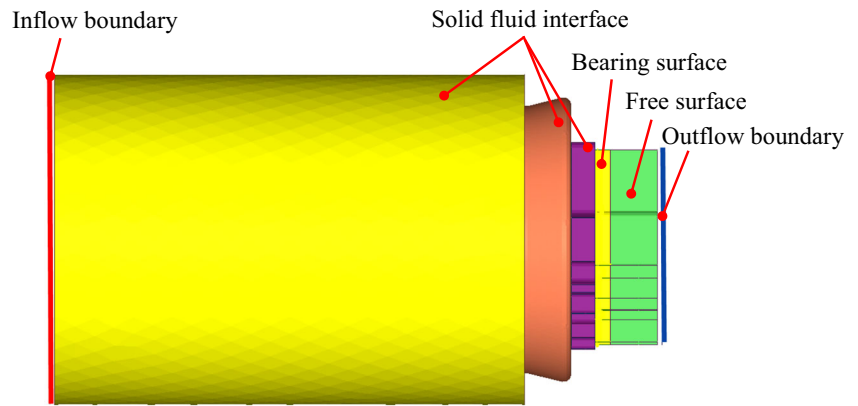
$$\rho \frac{\partial e_i}{\partial t} \Big|_{\xi} + \rho w_i \frac{\partial v_i}{\partial \xi_i} = T_{ji} \frac{\partial v_i}{\partial \xi_j} - \frac{\partial q_i}{\partial \xi_i} \quad (3)$$

where ρ , e_i , and f_i are the density, internal energy, and body force of unit mass; ξ_i and ξ_j are the Euler coordinates, respectively; w_i and w_j are the velocities of particle in reference coordinate system, respectively; t is the time; q_i is the bulk viscosity resistance; v_i is the velocities of particle in space coordinate system; T_{ji} is the Lagrangian stress tensor. The series of equations above need to be discretized and assembled into

Table 1 Physical properties of materials for extruded profiles and extrusion tools

Physical properties	Density (Kg/m ³)	Young's modulus (GPa)	Poisson's ratio	Specific heat (J/(kg K))	Conductivity (W/(m K))	Coefficient of thermal expansion (1/K)
AA6063 alloy	2690	68.9	0.35	900	198	$1.0e^{-5}$
H13 steel	7870	210	0.35	460	24.3	-

Fig. 7 Definitions of contact boundary types in the FE model of spreading extrusion process



equation systems and then solved through iterative algorithm. In this work, FE simulations based on the ALE algorithm for the spreading extrusion process to manufacture the large-size, flat-wide, and multi-ribs aluminum profile were carried out using HyperXtrude software package.

Figure 6 shows the FE model for simulating the spreading extrusion process of initial die scheme. The model was built in the HyperXtrude 14.0 interface and consisted of FE mesh, material data, boundary conditions, and process parameters. The FE mesh was created starting from CAD data using Step file format. The whole region, where metal flows through the extrusion tools and space, was extracted to create five~six components, including the initial billet, spreading chamber, pocket, bearing, and extruded profile. Before generating the mesh, place the origin (0, 0, 0) such that $x = 0$ and $y = 0$ were the center of the die and $z = 0$ was the die face that was in

contact with the billet. To save the computational time and assure the accuracy of simulated results, different element types and sizes were assigned to five components, which was also in accordance with the magnitude of local deformation at different regions. Since the material near the die exit was mainly subjected to severe local deformation, the element type of pentagonal prism was utilized to mesh the components of bearing and profile. And six free nodes need to be placed between the opposite walls (profile thickness). However, the tetrahedral meshes with relatively coarse element sizes were used in the components of pocket, spreading chamber, and billet. The element sizes for the five components along the extrusion direction were 12.5, 3.5, 0.8, 0.25, and 1.0 mm, respectively. The total number of elements in the FE model was about 1,300,000. After meshing, the quality of all elements meets the following criteria: maximum aspect ratio, $TET4 < 8$, $PYRAMID5 < 12$; minimum angle $> 15^\circ$,

Table 2 Definition of different contact boundaries at the exterior and interior faces of domains

Region	Boundary type	Detailed descriptions
Dummy block	Inflow boundary	Dummy block temperature: 480 °C; Billet temperature: 480 °C; Extrusion speed: 3.0 mm/s
Container	Solid wall	Temperature Container: 430 °C; Friction = Pure stick; Heat transfer coefficient: 3000 W/m ² °C
Spreading pocket and flat faced dies	Solid wall	Dies temperature: 430 °C; Friction = Pure stick; Heat transfer coefficient: 3000 W/m ² °C.
Bearing	Bearing surface	Friction model = Viscoplastic; Friction coefficient = 0.3; Heat transfer coefficient: 3000 W/m ² .°C
Extruded profile	Free surface	Environment temperature: 25 °C; Convection coefficient: 20 W/m ² .°C
Profile exit	Outflow boundary	X, Y, Z traction = 0; Heat flux = 0; Pressure is checked and 0
Anterior faces between different regions	Interiorsurf	—

Table 3 Extrusion process conditions used for this profile

Process conditions	Extrusion speed (mm/s)	Tools temperature (°C)	Billet temperature (°C)	Billet diameter (mm)	Billet length (mm)	Extrusion ratio
Values	3	430	480	210	500	101.581

maximum angle $< 165^\circ$; minimum value for “tet collapse” for elements in spreading chamber and pockets is > 0.2 . The calculation time of FE model was about 12 h by using Lenovo C60 workstation with a 16 GB RAM and 16 cores CPU.

Material constitutive model is an important factor affecting the accuracy of FE simulation for spreading extrusion process. In this work, the materials of profile and extrusion tools were the commercial AA6063 alloy and H13 steel, respectively. Table 1 shows the physical properties of the two materials. A classical Sellars–Tegart’s equation [26] was used to describe the material deformation behavior and the relationship between flow stress and deformation parameters such as temperature, strain, and strain rate. The flow stress in the above model was expressed as the following:

$$\bar{\sigma} = \frac{1}{\beta} \sinh^{-1} \left(\frac{\bar{\epsilon}}{A} e^{Q/RT} \right)^{1/n} \quad (4)$$

where $\bar{\sigma}$ is the flow stress; β is the temperature-independent material parameter; A is a constant; n is the stress exponent; $\bar{\epsilon}$ is the effective strain rate; Q is the activation energy; R is the universal gas constant, and T is the absolute temperature. For AA6063 alloy used in FE simulations, the corresponding material constitutive parameters in Eq. 4 were listed as follows: $\beta = 4.0 \times 10^{-8} \text{ m}^2/\text{N}$; $A = 5.91 \times 10^9 \text{ s}^{-1}$; $Q = 1.416 \times 10^5 \text{ J/mol}$; $R = 8314 \text{ J/(mol k)}$; $n = 5.385$.

Thermal boundary conditions are also major factors to affect the precision of FE simulations. The HyperXtrude software solver requires that appropriate boundary conditions are specified on all the exterior boundary faces and interior faces of different components. The boundary conditions were created using a set of 2D elements defined on the boundaries and the data to be specified on these. In the FE model, the boundaries of domain were classified into the six regions: inflow, solid wall, bearing, free surface, and outflow and interiorsurf, as shown in Fig. 7. The friction type in the boundaries between the billet and container and spreading pocket and flat-faced dies is defined as pure stick friction due to the high hydrostatic pressure and temperature (Table 2). However, the friction type in the boundary between the billet and die bearing is specified as viscoplastic friction. The model is similar to Coulomb friction, and the main difference is that the shear stress is a function of pressure and flow stress. A value of 0.3 for the friction coefficient was set. Based on the existing literature, the heat-transfer coefficient between the billet and

extrusion tools and between the extrude profile and environment were 3000 and $20 \text{ W/m}^2 \text{ }^\circ\text{C}$, respectively [26]. Table 3 shows the extrusion process parameters used for this profile in practical production. The billet diameter and length were 210 and 500 mm, respectively. The extrusion ratio was 101.58, which is larger than common solid profiles. The initial temperatures of the billet and extrusion tools were 480 and $430 \text{ }^\circ\text{C}$, respectively.

3 Exit flow velocity analysis

The flow velocity distribution on the cross-section of die exit is the most important indicator for evaluating the billet through the spreading pocket die with uniform flow behavior. Figure 8 a shows the velocity distribution on the cross-section of die exit for initial die design. It is clear that the maximum and minimum velocities are 362.64 and 185.03 mm/s, respectively. There exits relatively large flow velocities at the part with multi-ribs (see part B), while the flow velocities at the left end of profile (see part A) are extremely low. The actual flow velocity (extrusion speed*extrusion ratio) at the die exit is 304.74 mm/s. Thus, it can be seen that the material flow velocity on the cross-section of die exit is severe nonuniform and the maximum and minimum velocities are far from the theoretical velocity. The inconsistent front end of extrudate (see Fig. 8b) in the experiment really reflects the flow velocity difference at die exit. To quantitatively evaluate the material flow behavior, the standard deviation of velocity (SDV) along the extrusion direction was introduced [26]. The smaller the

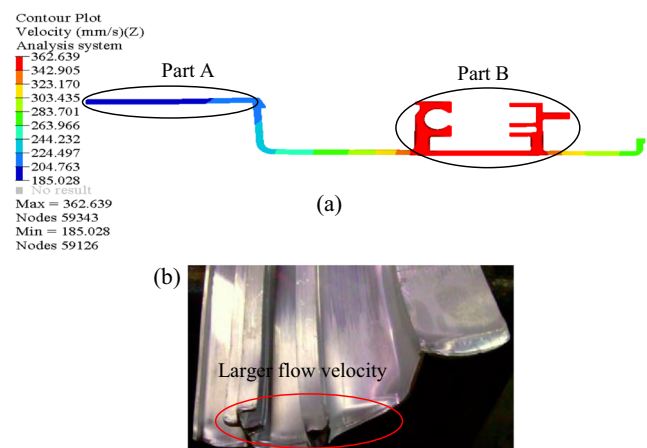


Fig. 8 a Velocity distribution on the cross-section of die exit for initial die design and b front end of extrudate in experiment

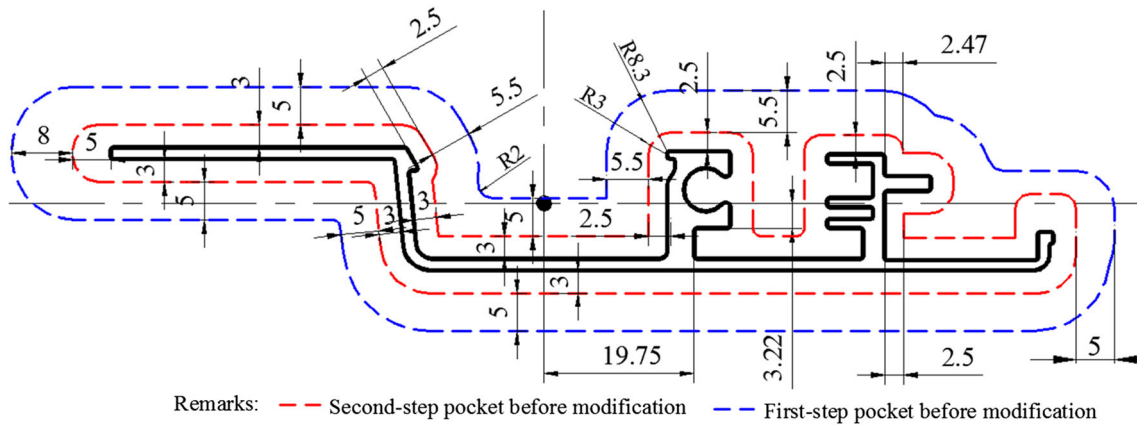


Fig. 9 The first modification scheme with adding a second-step pocket (unit:mm)

value of SDV, the more uniform the flow velocity distribution at the die exit will be. By extracting the velocities of all nodes on the cross-section of profile, the calculated SDV for the initial die design is up to 64.3 mm/s, which indicates a very poor velocity distribution. The main reasons for the nonuniform material flow are explained as follows: (1) the profile shape in part B is complex with multi-ribs and its section area and wall thickness is obviously larger than the other regions. As a result, the resistance of material flow from the container to die orifice during the whole extrusion process is minimum. (2) Part A is mostly located at the periphery of spreading pocket die and the position of die orifice is not placed at the central line of die. The material at the center of die flows faster than that of the outer edge. The farther the material away from the die center, the slower the material flow velocity. (3) There exists metal dead zones between the workpiece and die walls where the velocity is close to zero due to the strong sticking friction. The combination of these factors leads to the flow velocity in part A which is obviously slower than that in part B. Besides, the metal velocity differences along the extrusion direction are large, which further increase the difference in the metal supply at different section positions of profile.

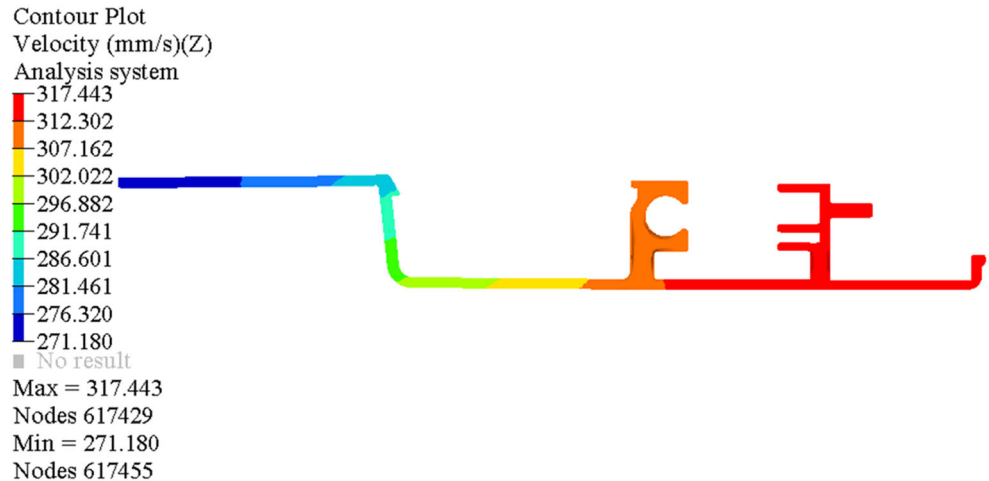
4 Balancing material flow through die structure optimization

One of basic design principles for spreading pocket die is that the billet is extruded through the die bearings with uniform flow velocity. Otherwise, a nonuniform flow distribution at die exit may lead to various extrusion defects in extruded profile such as distortion, bending, pitting, and waves and thicknesses thinning. Therefore, the initial die scheme is infeasible for the practical production of profiles. Some reasonable and effective methods should be adopted to optimize the geometric structure parameters of extrusion dies.

4.1 Adding pocket steps

Based on previous researches, single-step pocket die has a good effect on regulate material flow during extrusion process of solid profiles with simple cross-section or small length–width ratio [24]. However, it is very difficult to obtain a relative ideal for large length–width ratio and multi-ribs profiles using single-step pocket die. For the design of spreading pocket die, the number of pocket

Fig. 10 Velocity distribution on the cross-section of die exit with adding the pocket steps



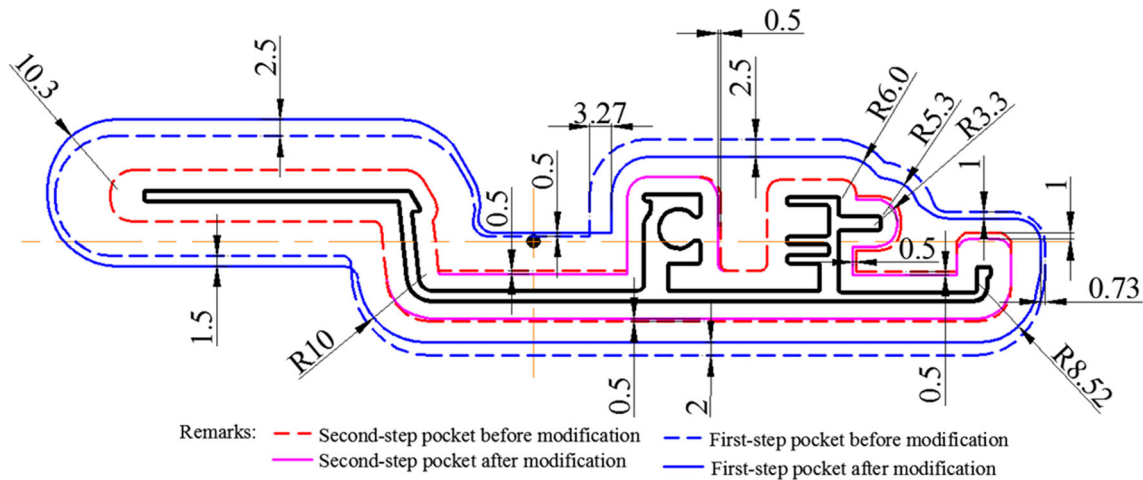


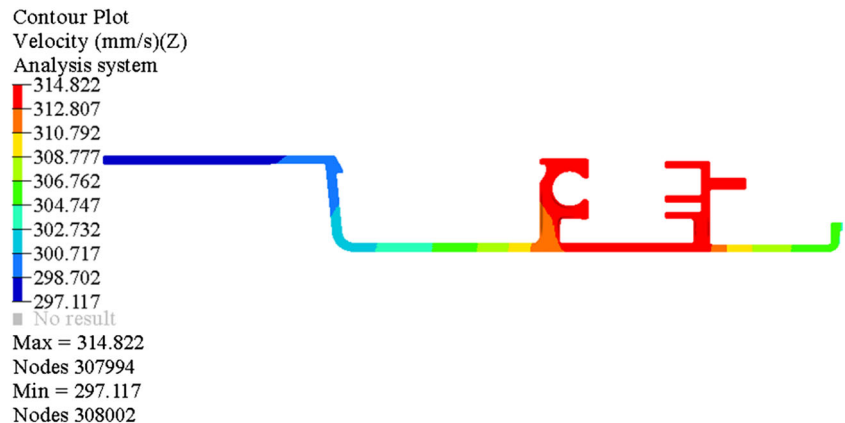
Fig. 11 Detailed modifications for the adjusting of the shape and dimension of multi-step pocket (unit:mm)

steps is one of the key geometrical parameters which has varied effects on material flow. The steps of pocket equate to increase the pocket angle, thus, making material flow easier, decreasing the dead metal zone in the pocket and lessening the flow nonuniformity [23]. Thus, in this study, double-step pockets were first adopted to adjust material flow during spreading extrusion. Figure 9 shows the outline and main dimensions of double-step pockets for the first modification scheme. The contours of first- and second-step pockets were similar. The distance between the first- and second-step pockets was designed to be 5–8 mm. The total depth of pockets was still 20 mm, and the depths of the first- and second-step pockets were 15 and 5 mm, respectively. With the extrusion by increasing the pocket steps, the velocity distribution on the cross-section of die exit is shown in Fig. 10. It can be seen that compared with initial die scheme, the maximum velocity decreased from 362.64 to 317.44 mm/s, while the minimum velocity increased from 185.03 to 271.8 mm/s. The maximum velocity difference reduced from 177.61 to 45.64 mm/s, and the calculated SDV decreased to 14.87 mm/s, which indicates that the material allocation and flow behavior during die cavity are greatly improved.

4.2 Adjusting the shape and dimensions of multi-step pockets

After adding the pocket steps, the velocity distribution uniformity on the cross-section of die exit in general is improved. However, the flow velocity at the multi-ribs and right end of profile is still very high, while at the left end of profile, it is relatively low. In the following, other modification methods should be utilized to decrease the flow velocity in these parts. The shape and dimensions of the multi-step pockets have important influence on material flow and product quality. According to the simulated results of the first modification (see Fig. 10), the shape and dimension of the first- and second-step pockets were adjusted in this modification scheme artificially. To balance the material flow, the dimensions of pockets at the multi-ribs and right end of profile are decreased, while at the left end of profile, they are increased. Figure 11 shows the detailed modifications for the adjusting of the shape and dimensions of pockets. The spread extrusion process was simulated again adopting the same process parameters as in the initial FE model. The obtained velocity distribution on the cross-section of die exit is shown in Fig. 12. It is clear that the maximum velocity further decreased

Fig. 12 Velocity distribution on the cross-section of die exit with adjusting the shape and dimension of multi-step pockets



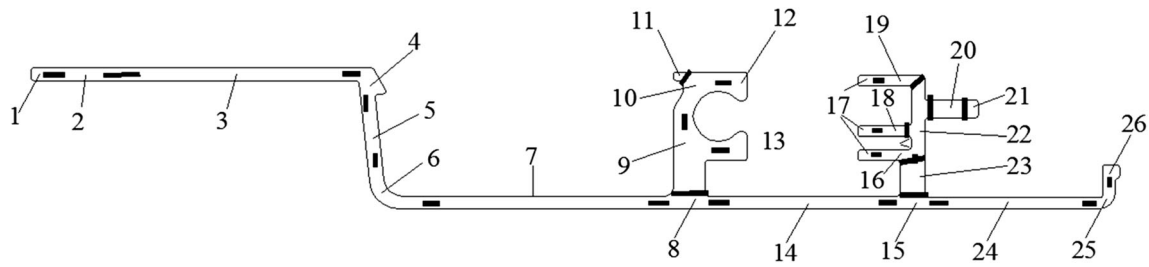


Fig. 13 The definition of bearing numbers for the initial and modified dies

to 314.82 mm/s and the minimum velocity increased to 297.12 mm/s. The calculated SDV is 9.43 mm/s, which is 35.58% lower than that of the first modification scheme. Owing to the effective balance of metal flow, the flow velocity in left end of profile increases greatly.

4.3 Optimizing bearing lengths

Although the above two modification schemes have effectively regulated the material flow behavior, it still cannot achieve precise control. Therefore, further adjustment of bearing lengths is adopted to balance the material flow velocity. The length of die bearings is one of the most important geometric parameters in the design of extrusion die, which is also the last “gate” to control the material through the die orifice with uniform velocity. The quality of final extruded products is directly dependent on the arrangement of bearing lengths at die orifices. The die bearing has negative effect on the metal flow. With the increase of bearing length, the metal flow resistance due to the additional slip friction and hydrostatic pressure from the supplied metal increases which enforces the metal to flow into the orifice with less flow resistance. In order to determine the lengths of die bearings reasonably, two main factors should be considered, i. e., the arrangement of die orifices and the wall thickness of each parts of the profile. In general, the two ends of profile farthest from the container center are selected as design baselines of die bearings where the length should be designed to minimum. Then, the bearings’ lengths of the other regions are determined according to the distance between the die orifice and die center and the wall thicknesses of parts of profile. Based on the abovementioned

design principle, the bearing lengths in the die orifices were artificially adjusted for several times and a relatively perfect result is finally achieved. Figure 13 and Table 4 show the definition of bearing numbers for the initial and modified dies and the adjustments from the initial to modified dies. The simulation result of exit velocity distribution is shown in Fig. 14. It can be seen that the maximum and minimum velocities are 306.24 and 302.81 mm/s, respectively, which are almost close to the actual velocity with a value of 304.74 mm/s. The maximum velocity difference is only 3.34 mm/s, and the calculated SDV value is as low as 0.92 mm/s.

5 Comparisons between initial and modified die schemes and experimental verification

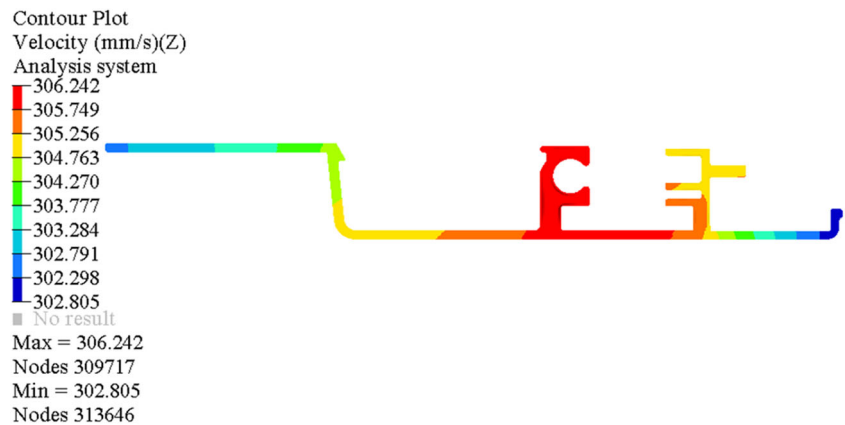
5.1 Material flow behavior

To reveal the material flow behavior through the spreading pocket and flat-faced dies during extrusion, several sections that cut the workpiece along the extrusion direction were extracted. Figure 15 shows the material flow behavior during spreading extrusion for the initial and modified dies, which characterized the flow path of material from the container to the final product. It can be seen that for the initial die design (Fig. 15a), the material flow in the exit of the spreading chamber is severely nonuniform, and the velocities in the two ends of pocket is close to zero (red and blue color represent the maximum and minimum velocities, respectively). When material flows through the pocket, the velocity difference on the cutting section is further increased. As a result, an uneven flow

Table 4 The length of bearings in the initial and modified die schemes (unit:mm)

Bearing number	1	2	3	4	5	6	7	8	9	10
Initial design (mm)	1.6	2.9	3.3	4.2	4	2.6	3.2	5	8.5	5
Modified design (mm)	1.4	2.5	3.0	4.2	4	2.6	3.2	6	10	7.5
Bearing number	11	12	13	14	15	16	17	18	19	20
Initial design (mm)	2	2.5	2.5	3	5	1.7	1.1	1.7	1.9	4.9
Modified design (mm)	4.5	3	3	4.5	6	5	1.1	5	4.5	5
Bearing number	21	22	23	24	25	26				
Initial design (mm)	2.5	4	8.3	2.7	1.9	1.2				
Modified design (mm)	2.5	6	10	2	1.6	1.1				

Fig. 14 Velocity distribution on the cross-section of die exit with optimizing the bearing lengths



velocity will cause the difference in the front end shape of extruded profile, which brings about the length in the part of multi-ribs being longer than those of the other parts. It can be seen from Fig. 15 b that material flow velocities in each extracted section are basically the same, which indicates that the material allocation and flow behavior in the spreading pocket die are almost reasonable. Table 5 shows the detailed comparisons of maximum velocity difference, SDV, and the difference in the front end of extruded profile for the initial and optimal dies. It is clear that the maximum velocity difference and SDV respectively decreased from 177.61, 64.3 mm/s to 3.44, 0.92 mm/s. The front end shape difference of extruded profile for the optimal die is 1.08 mm, which is reduced by 18.02 mm.

5.2 Temperature field at die exit

The uniformity of microstructure and mechanical properties for extruded products is mainly dependent on the temperature distribution on the cross-section of profile at die exit. The main factors affecting the temperature variation of billet during spreading extrusion include plastic deformation heat, friction heat, and heat transfer between workpiece and extrusion tools. Among them, the temperature distribution on the cross-section of die exit is mainly influenced by the plastic deformation heat and friction heat produced by the billet through the spreading pocket die. Figure 16 shows the temperature distribution on the cross-section of die exit for the initial and modified dies. It can be seen that the minimum temperature for the initial die is located at the left end of profile and the value is 511.23 °C, while the maximum temperature with a value of 529.1 °C is located at the center section. The maximum temperature difference over the cross-section of profile is up to 17.87 °C. Although strong friction exists between the workpiece and wall of pocket die, the plastic deformation heat at the left end of profile is much lower than that of other parts due to the severe nonuniform plastic deformation of the billet. After optimizing the die structure, the material flow behavior

during spreading pocket die is better and the uniformity of plastic deformation is also improved. Thus, a reasonable control of plastic deformation heat and friction heat between workpiece and extrusion tools is achieved. The maximum temperature difference over the cross-section of profile decreased from 17.87 to 9.48 °C, which greatly improves the nonuniform distribution of exit temperature. The uniformity of temperature distribution is conducive to obtaining uniform microstructure and mechanical properties of extrudate.

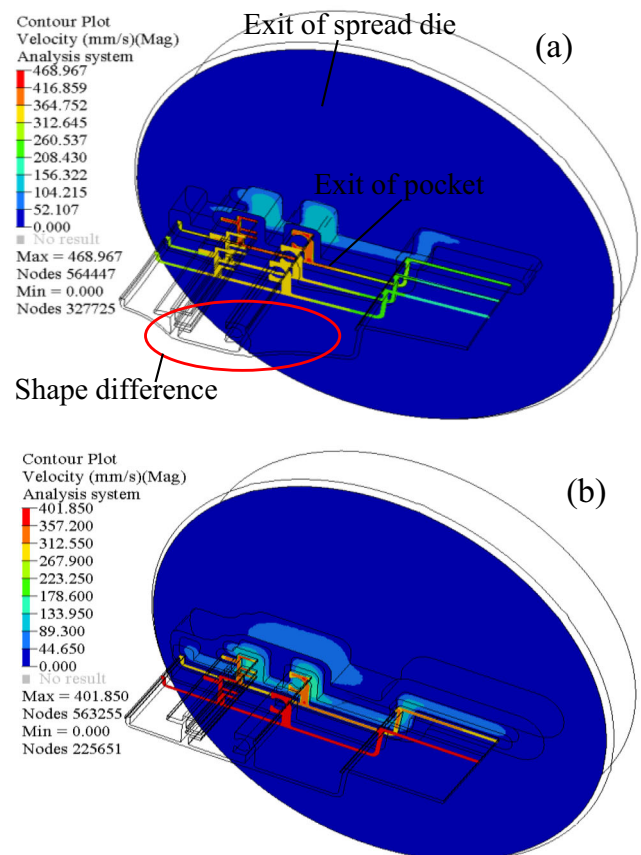


Fig. 15 Material flow behavior during spreading extrusion process. **a** Initial die. **b** Modified die

Table 5 Detailed comparisons of maximum velocity difference, SDV, and the difference in the front end of extruded profile for the initial and modified dies

Die scheme	Minimum velocity (mm/s)	Maximum velocity (mm/s)	Maximum velocity difference (mm/s)	SDV (mm/s)	Difference in the front end shape of extruded profile (mm)
Initial die	185.028	362.639	177.611	64.3	19.1
Modified die	302.805	306.242	3.437	0.92	1.08

5.3 Stress and strain distributions of billet during extrusion

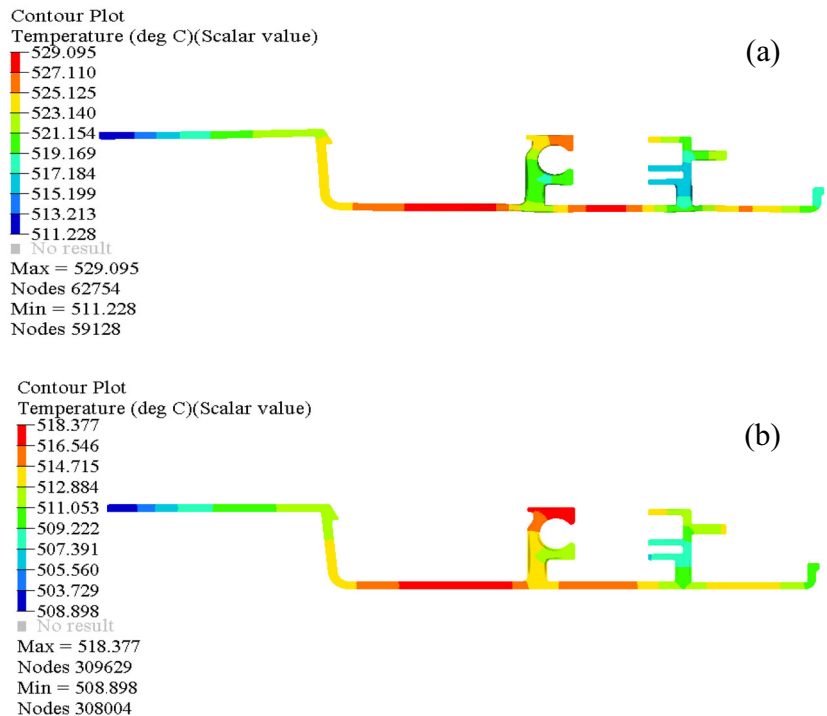
Figure 17 a shows the stress distributions of billet for the initial and modified dies. It can be seen that the von Mises stress increases slightly along the extrusion direction, then reaches to a maximum at the die orifices where the local shear deformation is severe, and finally decreased to low value at die exit. The von Mises stress at the dead metal zone of spreading chamber is close to zero. For the initial die, the stress distribution at the pocket is severely nonuniform. The minimum stress is located at the right side of pocket with a value of about 20 MPa. After optimization, a uniform stress distributions at first- and second-pockets are obtained. Figure 17 b shows the effective strain distributions at die cavity for the initial and modified dies. The strain in the spreading chamber is less than 5 due to the low plastic deformation. Once the metal flows into the pocket, the strain increases rapidly to a large value. At the corner of pockets, the stain is almost zero. For the initial die, the strain value at the part with

multi-ribs is obviously less than that of the other regions. And the strain value at the die orifices is at a range of 30~50. For the optimized die, the plastic deformation in the second-step pocket and die orifices is homogeneous.

5.4 Residual stresses in extrudate

The residual stress distribution of extrudate is a key factor to the stability of shape and position accuracy and mechanical performance. The large and uneven residual stress distribution causes extrudate deformation to be more complex during subsequent heat treatment process and decreases the production efficiency and accuracy. Therefore, the study of residual stress of extrudate has great engineering value. A proper die design can decrease significantly the residual stress in extrudate. After extrusion, large residual stress is mainly caused by the nonuniform temperature and velocity distributions of each part of profile cross-section. On the one hand, thermal stress is caused by the large temperature difference of profile section; on the other hand, the parts with high material flow

Fig. 16 Temperature distribution on the cross-section of die exit. **a** Initial die. **b** Modified die



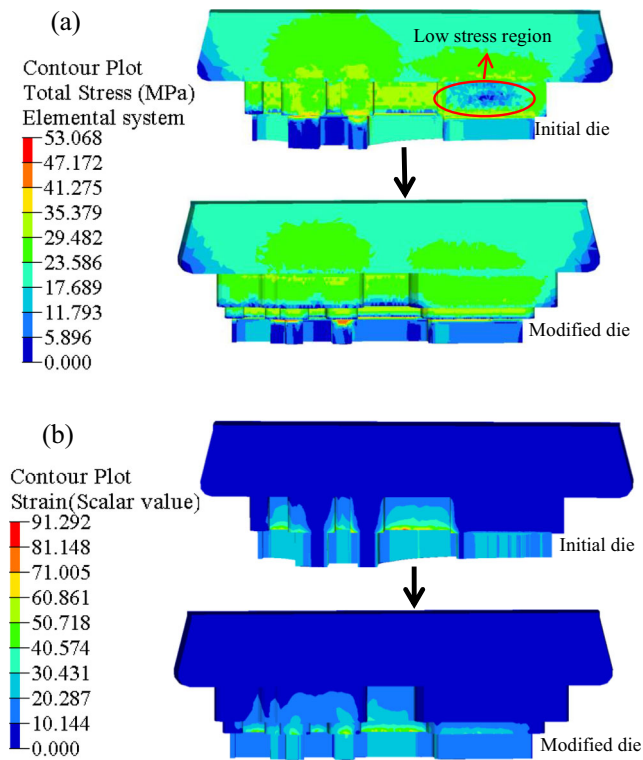


Fig. 17 Stress and strain distributions of billet during extrusion for initial and modified dies. **a** Stress distribution. **b** Strain distribution

velocity will lead to high tensile stress. Figure 18 shows the residual stress distributions of extrudate for the initial and modified dies. It can be seen that there exists large residual tensile stress at the joints between the multi-ribs and main panel, and the maximum value is up to 28.1 MPa. This is

Fig. 18 Residual stress distribution of extrudate. **a** Initial die. **b** Modified die

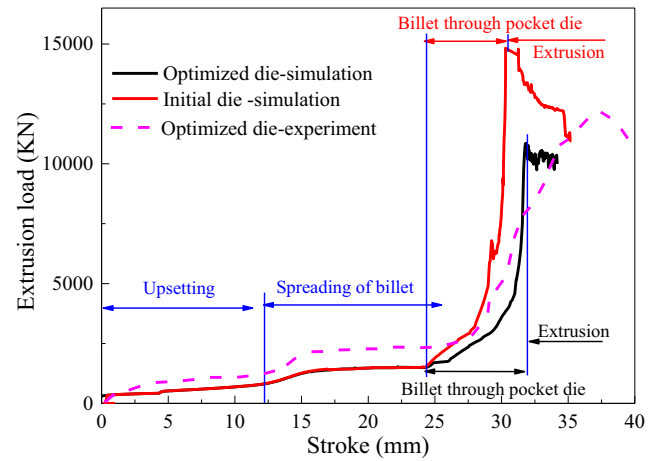
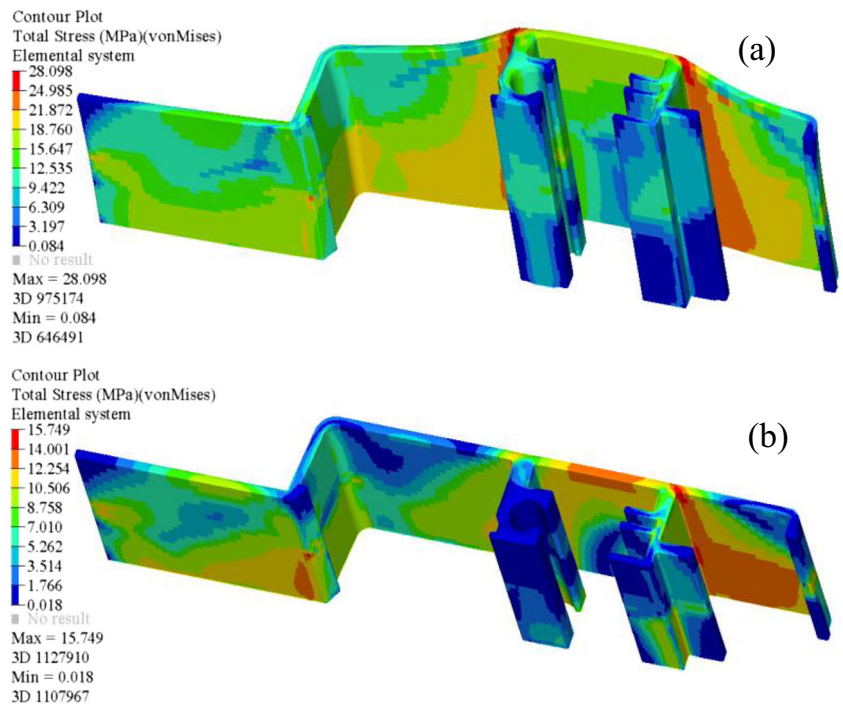


Fig. 19 Extrusion force required for extruding the billet through spreading pocket die for the initial and modified schemes

mainly due to the metal in the multi-ribs of extrudate flows obviously faster than that in the other parts of extrudate (see Fig. 8). Correspondingly, the metal in the multi-ribs suffers larger tensile stress, while in the other parts of extrudate, suffers compressive stress. Moreover, there exists a certain degree of heat stress at the center section of profile. After a series of modifications for spread pocket die, the maximum residual stress decreased to 15.75 MPa.

5.5 Peak extrusion force

Extrusion force is also an important index for reasonably formulating process regulations, accurately determining the capacity of extrusion press, and designing the extrusion tools.

Fig. 20 Extrusion dies for actual production of aluminum profiles. **a** Spreading pocket die. **b** Flat-faced die

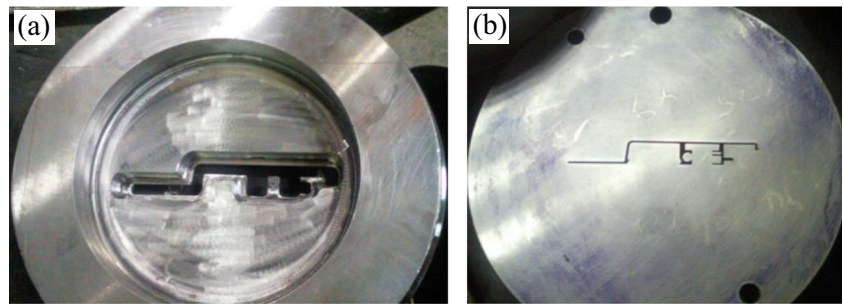


Figure 19 shows the variation of extrusion force with the stroke of dummy block during the whole spreading extrusion process for the initial and modified dies. It can be seen that the extrusion force experiences four obvious stages: in the first stage of the upsetting of billet, the extrusion force is relatively low, and the value is lower than 800 KN; in the second stage, the billet is spread with an external diameter which is far larger than that of the profile. And the extrusion force increased to 1500 KN; in the third stage, the spreading billet is enforced flowing through the chamber of pocket die. The extrusion force increases significantly until reaching a peak value in which the local deformation is maximum. In the last stage, the billet is extruded through the die bearing to form the final product. As a result, the extrusion force decreases gradually. It can be also seen from Fig. 19 that the extrusion force for the initial die with a value of 14,780 KN is obviously larger than that of the modified die with a value of 10,644 KN. Although the total contact surface between the billet and spreading pocket die for the initial die is less than that of the modified die with two-step pockets, the increase of pocket steps improves greatly the material flow uniformity in spread extrusion process. Thus, the billet is easier to extrude out of the die orifice, thereby reducing the extrusion force. Besides, the extrusion load curve for the modified die in general agrees relatively well with experimental one. The peak extrusion load in the experiment is 1516 KN more than the simulated one.

5.6 Verification by extrusion experiments

To verify the rationality of virtual die tryout technology based on FE simulations, the modified extrusion dies were manufactured (see Fig. 20) and corresponding extrusion experiments were carried out on the horizontal extrusion press.

Fig. 21 Sample of the large-size, flat-wide, and thin-walled aluminum profile using optimal die



The process parameters adopted in the real extrusion production were exactly the same as the FE simulations, and the actual extruded profile is shown in Fig. 21. It is clear that there are no obvious extrusion effects such as bending, twisting, and cracking. The vernier calipers and micrometers were used to measure the overall dimensions and wall thickness. Length and width dimensional errors smaller than 0.2 mm and wall thickness difference less than 0.1 mm were found in the extruded profile. The surface finishment also meets the quality requirements. Besides, three representative positions on the cross-section of profile were chosen to further investigate the homogeneity of mechanical properties of extruded profile, as shown in Fig. 22. All samples were taken from the marked positions of extruded profile along the extrusion direction. The gauge length and width of tensile samples were 46 and 12.5 mm, respectively. The tensile tests were carried out at a tensile rate of 2 mm/min using an Instron-type electrochemical machine and were repeated three times for each position to ensure the accuracy and repeatability of the tests. It can be seen from Fig. 22 that the yield strength of samples 1, 2, and 3 are respectively 152.2, 163.5, and 164.1 MPa, and corresponding tensile strengths are 229.0, 230.15, and 222.7 MPa, which indicate that the deformation microstructure and grain sizes on the cross-section of profile are basically identical from a side view. This is largely due to the modified die that allocates the material reasonably in die cavity and improves significantly the flow velocity uniformity at die exit, resulting in a uniform temperature field on the cross-section of profile. This work demonstrates the feasibility of using ALE simulations as an effective tool to design and optimize the spreading pocket die in the actual production of large-size, flat-wide, and multi-ribs extruded profiles.

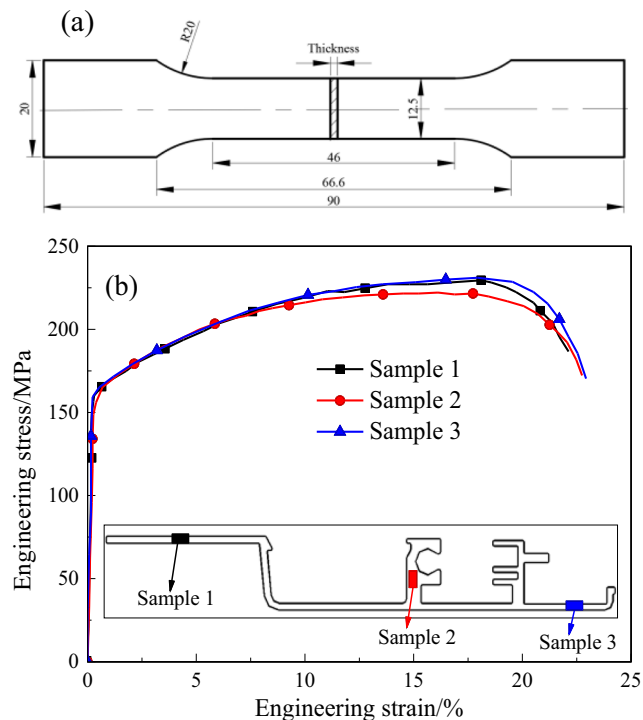


Fig. 22 Dimension of tensile samples and stress–strain curves of extruded profile at different positions. **a** Dimension of tensile sample (unit:mm). **b** Engineering stress–strain curves

6 Conclusions

In this study, virtual tryout of spreading extrusion process for a large-size, flat-wide, and multi-ribs aluminum profile was performed through numerical simulation. The material flow uniformity on the cross-section of die exit was evaluated quantitatively by using the SDV. Then, three-step modifications for the spreading pocket die were proposed to optimize the material flow during die cavity. Moreover, a synthetical comparison of extrusion formability for the modified and initial die schemes was carried out. Finally, the modified extrusion dies were manufactured, and extrusion experiment was performed to verify the effectiveness and reliability of FE simulations. The obtained conclusions are drawn as follows:

- The calculated SDV for the initial die design is up to 64.3 mm/s, which indicates a very poor velocity distribution. There exists relatively large flow velocity at the part with multi-ribs, while the flow velocity at the left end of profile is extremely low. This is mainly attributed to the combined effects of the differences of wall thicknesses of profile and the positions of die orifices and metal dead zones.
- After three modifications for spreading pocket die, perfect flow velocity distribution on the cross-section of die exit with SDV of 0.92 mm/s is obtained. Moreover, more uniform temperature distribution on the cross-section of

profile, lower residual stresses in extruded profile, and lower required extrusion force are achieved.

- The key design points of spreading pocket die for the large-size, flat-wide, and multi-ribs aluminum profile are proposed, which include adding the pocket steps, adjusting the shape and dimensions of multi-step pockets, and optimizing the die bearings.
- The high dimensional accuracy and relatively consistent mechanical properties of extruded profile proved the validity of die design method based on ALE simulation for the spreading extrusion of large-size and flat-wide solid profiles.

Funding information The authors gratefully acknowledge the research support from the National Natural Science Foundation of China (grant no. 51605234), Hunan Provincial Natural Science Foundation of China (grant no. 2019JJ50510), Scientific Research Fund of Hunan Provincial Education Department (grant no. 18B285), and the Opening Project of Cooperative Innovation Center for Nuclear Fuel Cycle Technology and Equipment, University of South China (grant no. 2019KFY06).

References

1. Yi J, Wang ZH, Liu ZW, Zhang JM, He X (2018) FE analysis of extrusion defect and optimization of metal flow in porthole die for complex hollow aluminium profile. *Trans Nonferrous Met Soc China* 28(10):2094–2101
2. Ji H, Nie H, Chen W, Ruan X, Pan P, Zhang J (2017) Optimization of the extrusion die and microstructure analysis for a hollow aluminium alloy profile. *Int J Adv Manuf Technol* 93(9–12):3461–3471
3. Qamar SZ, Chekotu JC, Al-Maharbi M, Alam K (2019) Shape complexity in metal extrusion: definitions, classification, and applications. *Arab J Sci Eng* 44(9):7371–7384
4. Velay X (2009) Prediction and control of subgrain size in the hot extrusion of aluminium alloys with feeder plates. *J Mater Process Tech* 209(7):3610–3620
5. Li Q, Smith CJ, Harris C, Jolly MR (2003) Finite element investigations upon the influence of pocket die designs on metal flow in aluminium extrusion: part I. effect of pocket angle and volume on metal flow. *J Mater Process Tech* 135(2–3):189–196
6. Fang G, Zhou J, Duczczek J, Wu XK (2008) FE simulation of extrusion to produce a thin-walled wide profile through a spreading pocket die. *Key Eng Mater* 367:63–70
7. Xie JX, Murakami T, Ikeda K, Takahashi H (1995) Experimental simulation of metal flow in porthole-die extrusion. *J Mater Process Tech* 49(1–2):1–11
8. Tiernan P, Hillery MT, Draganescu B, Gheorghe M (2005) Modelling of cold extrusion with experimental verification. *J Mater Process Tech* 168(2):360–366
9. Gordon WA, Van Tyne CJ, Sriram S (2002) Extrusion through spherical dies—an upper bound analysis. *J Manufac Sci Eng* 124(1):92–97
10. Farzad H, Ebrahimi R (2016) Die profile optimization of rectangular cross section extrusion in plane strain condition using upper bound analysis method and simulated annealing algorithm. *J Manufac Sci Eng* 139(2):021006
11. Jiang Y, Wu R, Yuan C, Wang W, Jiao W (2019) Prediction and analysis of breakthrough extruding force based on a modified FE-model in large-scale extrusion process. *Int J Adv Manuf Technol* 104(9–12):3531–3544

12. Ikumapayi OM, Oyinbo ST, Bodunde OP, Afolalu SA, Okokpujie IP, Akinlabi ET (2019) The effects of lubricants on temperature distribution of 6063 aluminium alloy during backward cup extrusion process. *J Mater Res Technol* 8(1):1175–1187
13. Liu Z, Li L, Yi J, Li S, Wang G (2017) Influence of extrusion speed on the seam weld quality in the porthole die extrusion of AZ31 magnesium alloy tube. *Int J Adv Manuf Technol* 92(1–4):1039–1052
14. Ammu VV, Mahendiran P, Agnihotri A, Ambade S, Dungore PR (2018) A simplified approach for generation of bearing curve by velocity distribution and press validation for aluminum extruded profile. *Int J Adv Manuf Technol* 98(5–8):1733–1744
15. Gagliardi F, Ciancio C, Ambrogio G (2018) Optimization of porthole die extrusion by Grey-Taguchi relational analysis. *Int J Adv Manuf Technol* 94(1–4):719–728
16. Xue X, Vincze G, Pereira A, Pan J, Liao J (2018) Assessment of metal flow balance in multi-output porthole hot extrusion of AA6060 thin-walled profile. *Metals* 8(6):462
17. Pan JY, Xue X (2018) Numerical investigation of an arc inlet structure extrusion die for large hollow sections. *Inter J Mater Form* 11(3):405–416
18. Wang D, Zhang C, Wang C, Zhao G, Chen L, Sun W (2018) Application and analysis of spread die and flat container in the extrusion of a large-size, hollow, and flat-wide aluminum alloy profile. *Int J Adv Manuf Technol* 94(9–12):4247–4263
19. Imamura Y, Takatsuji N, Matsuki K, Tokizawa M, Murotani K, Maruyama H (1999) Metal flow behaviour of wide flat bar in the spreading extrusion process. *Mater Sci Technol* 15(10):1186–1190
20. Yan H, Xia J (2006) An approach to the optimal design of technological parameters in the profile extrusion process. *Sci Technol Adv Mater* 7(1):127–131
21. Abrinia K, Makaremi M (2009) An analytical solution for the spread extrusion of shaped sections. *Int J Adv Manuf Technol* 41(7–8):670–676
22. Liu Z, Li L, Yi J, Wang G (2019) Entrance shape design of spread extrusion die for large-scale aluminum panel. *Int J Adv Manuf Technol* 101(5–8):1725–1740
23. Fang G, Zhou J, Duszczek J (2008) Effect of pocket design on metal flow through single-bearing extrusion dies to produce a thin-walled aluminium profile. *J Mater Process Tech* 199(1–3):91–101
24. Zhang C, Yang S, Zhang Q, Zhao G, Lu P, Sun W (2017) Automatic optimization design of a feeder extrusion die with response surface methodology and mesh deformation technique. *Int J Adv Manuf Technol* 91(9–12):3181–3193
25. Martins MM, Button ST, Bressan JD (2016) Analysis of aluminum extrusion in a 90° die by finite volume method. *Adv Mater Res* 1135:153–160
26. Liu Z, Li L, Li S, Yi J, Wang G (2018) Simulation analysis of porthole die extrusion process and die structure modifications for an aluminum profile with high length–width ratio and small cavity. *Materials* 11(9):1517

Publisher's note Springer Nature remains neutral with regard to jurisdictional claims in published maps and institutional affiliations.